Supplementary Information (SI) for Physical Chemistry Chemical Physics.

Supplemental Information: Direct in situ Detection of Grain Boundary Reduction in Nanocrystalline Ceria

Claire M. Donahue[1], Qing Ma[2], and Sossina M. Haile[1,*]

[1]Department of Materials Science and Engineering, Northwestern University, Evanston, IL, 60208, USA

[2]Dow-Northwestern-Dupont Collaborative Access Team, Synchrotron Research Center

*sossina.haile@northwestern.edu

Self-absorption adjustment in linear combination fitting

Linear combination fitting is a method by which linear combinations of reference spectra with elements in known oxidation states are weighted and summed to match the observed spectra. The relative weights are then used to determine the average oxidation state. In sufficiently thin films (or short path lengths through a sample), self-absorption effects can be ignored. In the limit of measurements performed at incidence angles below ~⅔ of the critical angle (~0.45°), no self-absorption is expected [1]. Accordingly, in the present study, self-absorption effects are absent in the surface measurement (α = 0.23°). In the full-film measurements, which include the Ce^{3+} and Ce^{4+} reference spectra, self-absorption effects are limited, but non-negligible. These minor effects are accounted for via the following treatment.

The measured (or observed) normalized absorption spectrum (μ) is related to the true absorption spectrum (μ_{true}) according to

$$\mu(E) = \frac{\frac{\mu_{true}}{\mu_{true}+A}\left(1-\exp\left(-\frac{B}{A}\mu_{true}-B\right)\right)}{\frac{1}{1+A}\left(1-\exp\left(-\frac{B}{A}-B\right)\right)} \quad \text{(S1)}$$

where *A* and *B* are positive dimensionless quantities that describe the details of the sample, beam, and measurement geometry [2]. The true absorption spectrum, μ_{true}, can be described as a linear combination of self-absorption-free reference spectra:

$$\mu_{true}(E) = (c')\,\mu_{true,Ce^{3+}}(E) + (1-c')\,\mu_{true,Ce^{4+}}(E) \quad \text{(S2)}$$

where c' is the quantity of interest, the fraction of absorbing Ce atoms which are in the 3+ oxidation state. To determine c', one requires not only knowledge of the *A* and *B* parameters to obtain μ_{true} from the measured μ, but also reference spectra that are entirely free of self-absorption effects. Because it was not possible to determine the parameters nor to obtain ideal reference spectra entirely free of absorption effects, a modified analysis approach was pursued.

Conveniently, the functional form of the absorption spectrum given in equation S1 has the property of satisfactorily describing observed spectra even when the reference spectra ($\mu_{Ce^{3+}}$, $\mu_{Ce^{4+}}$) suffer from self-absorption effects. In this case, however, the *A* and *B* quantities lose their direct physical meaning, and negative values of *A* can account for situations in which the reference spectra are more impacted by self-absorption than the sample spectra. Within this formalism, we define μ_{LC} as the linear combination of the measured reference spectra according to

$$\mu_{LC}(E) = (c')\,\mu_{Ce^{3+}}(E) + (1 - c')\,\mu_{Ce^{4+}}(E) \tag{S3}$$

and insert μ_{LC} in place of μ_{true} in equation S1 to arrive at an overall expression for the observed spectrum:

$$\mu(E) = \frac{\frac{c'\mu_{Ce^{3+}} + (1-c')\mu_{Ce^{4+}}}{c'\mu_{Ce^{3+}} + (1-c')\mu_{Ce^{4+}} + A}\left(1 - \exp\left(-\frac{B}{A}(c'\mu_{Ce^{3+}} + (1-c')\mu_{Ce^{4+}}) - B\right)\right)}{\frac{1}{1+A}\left(1 - \exp\left(-\frac{B}{A} - B\right)\right)} \tag{S4}$$

$\mu(E)$ is fitted to the experimental data, $\mu_{obs}(E)$, to determine c', and *A* and *B* are arbitrary fitting parameters.

Figure 2 shows fitting results for each of the five measurements in this work. In Table S1 and Figure S5, we compare the complete fitting model which accounts for self-absorption ("LC + SA") to a simpler linear combination fitting method ("LC only") in which equation S3 is used as the fitting model. When self-absorption effects in reference and experimental spectra are comparable, conventional LC fitting produces satisfactory results. When the mismatch is considerable, however, as is the case for the surface XANES measurement, conventional LC fitting is unable to capture the features of the measured spectra. Accordingly, in the full-film measurements, the conventional and self-absorption-corrected approaches yield comparable c' values and uncertainties. In the surface measurement, because the self-absorption effects in the reference and experimental spectra are significantly different due to differing measurement geometries, the conventional approach yields a significantly poorer fit and a value of c' with higher uncertainty.

For the purpose of visualizing experimental XANES spectra in comparison to reference spectra, where these two types of spectra have differing self-absorption effects, the two experimental spectra in Figure 3 are reconstructed using the fitted *A* and *B* parameters such that the effective degree of self-absorption is consistent with the references. In Figures 2 and S5, this minor adjustment has not been applied and the original normalized XANES data for each measurement are shown.

Characterization of surface reduction and determination of $c_{film\ bulk}$ in single-crystal CeO_2

In X-ray absorption spectroscopy, the exponential decay with depth, z, of the X-ray beam in the sample is characterized by a penetration depth, Λ, the depth at which the X-ray intensity decays to 1/e of that at the surface. A single XANES measurement can only yield a single value c', the fractional Ce^{3+} character of the spectrum obtained by LC fitting, that reflects the Ce^{3+} concentration profile in the material, $c(z)$. Simple exponential decay defined by Λ in a material with dimension L on the z axis implies the following equation:

$$c' = \frac{1}{\Lambda\left(1 - \exp\left(-\frac{L}{\Lambda}\right)\right)} \int_0^L c(z) \exp\left(-\frac{z}{\Lambda}\right) dz \qquad (S5)$$

The profile $c(z)$ is not known, but literature studies indicate that the near-surface enrichment of Ce^{3+} drops off steeply with depth. Since the exact features of $c(z)$ are not the focus of the present study, we approximate the profile using a step function, where $c(z)$ consists of a fully-reduced surface region, $c\left(z \le \ell_{surf}\right) = 1$, and a bulk-like region, $c\left(z > \ell_{surf}\right) = c_{film\ bulk}$. While reduction at the film-substrate interface is possible, we ignore any such effect due to the low contribution of this deep region in the film to the measured signal.

By inserting this piecewise step-profile function for $c(z)$, solving the integrals analytically, and rearranging into an expression for ℓ_{surf}, equation S5 reduces to the following:

$$\ell_{surf} = -\Lambda \ln\left(\frac{1 - c' + \left(c' - c_{film\ bulk}\right)\exp\left(-\frac{L}{\Lambda}\right)}{1 - c_{film\ bulk}}\right) \qquad (S6)$$

In principle, calculation of ℓ_{surf} for single-crystal ceria using this expression is straightforward because c' is obtained from LC fitting, Λ is determined by the X-ray incidence angle and material properties (discussed below), and $c_{film\ bulk}$ can be taken as the equilibrium concentration for the given experimental conditions (T and pO_2). In the present study, however, we treat $c_{film\ bulk}$ as unknown in order to extract it from the experimental data and validate our methods. For this, it is possible to determine ℓ_{surf} and $c_{film\ bulk}$ simultaneously with the use of two measurements in the same condition with different penetration depths (and hence different c' values). These values are available from the two XANES measurements of the single-crystal CeO_2 film in condition #2: (1) full-film XANES, α = 9.5°, Λ ~ 500 nm, c' = 0.047 (Figure 2.d, 3); (2) surface XANES, α = 0.23°, Λ = 2.6 nm, c' = 0.557 (Figure 2.e). Inserting each set of values into equation S6 yields a system of two equations, which we then solve numerically for ℓ_{surf} and $c_{film\ bulk}$.

We determine ℓ_{surf} = 2.0 nm and $c_{film\ bulk}$ = 3.6% for the single-crystal CeO_2 film in condition #2. The $c_{film\ bulk}$ value is very close to the TGA prediction of 3.7% for the nominal *T* and pO_2 of this condition (Figure 4), confirming accurate environmental control in these experiments.

Λ = 500 nm is an approximate value for the full-film XANES measurement calculated for α = 9.5°, using tabulated scattering factors for CeO_2, and an arbitrary X-ray energy near the Ce L_3 edge; we do not require a precise value since equation S6 is largely insensitive to small variations in Λ when Λ is large (compared to L). In surface-sensitive XANES, however, the value of Λ is important and, moreover, its variation with energy near the absorption edge is considerable. Here, we calculated $\Lambda(E)$ (not shown) directly from the measured absorption fine structure (Figure 2.e) by a method detailed elsewhere [3]. While $\Lambda(E)$ varies with energy, ranging between approximately 2.35 and 2.95 nm across the fitting range, we deem it appropriate to assign a single value of Λ = 2.6 nm, corresponding to the value at 5728.4 eV (the energy of coincidence of Ce^{3+} and Ce^{4+} reference spectra).

Alternative approach to estimate conductivity enhancement

To estimate conductivity enhancement due to grain boundary reduction in this study, approximate upper-bound enhancement factors were reported in the main text through an approach which assumes a uniform Ce^{3+} spatial distribution. Here, we approximate the Ce^{3+} distribution in the nanocrystalline CeO_2 film by the brick-layer model and use bulk electronic conductivity data [4], in conjunction with known and observed values ($c_{CeO_2\ bulk}$, $c_{film\ bulk}$, t_{grain}) in each of the three experimental conditions, to calculate the expected total conductivity. By applying bulk conductivity data to both grain interiors and grain boundaries, this approach assumes that conductivity effects in nanoceria are determined solely by spatial variation in Ce^{3+} concentration, neglecting the possibility that mobility near grain boundaries differs from bulk mobility. The approach provides a valuable comparison to the simpler analysis in the main text and corroborates the use of the latter analysis for an upper-bound estimate of conductivity enhancement.

The brick-layer model employed here consists of cubic grains with distinct interior and grain boundary features. The interior regions of the grains have side length $t_{grain} - \ell'_{GB}$ and Ce^{3+} concentration ($c_{CeO_2\ bulk}$) that matches the expected equilibrium value for the bulk [5]; the grain boundaries have a variable width ℓ'_{GB} and a variable Ce^{3+} concentration c_{GB}. The values of ℓ'_{GB} and c_{GB} are co-dependent according to the condition that the total Ce^{3+} concentration must equal the observed value ($c_{film\ bulk}$). In each of the three experimental conditions, $c_{CeO_2\ bulk}$ is fixed at its known thermodynamic value while c_{GB} and ℓ'_{GB} are co-varied in a manner representing different degrees of localization of the excess Ce^{3+} to grain boundaries. The grain interior and grain boundary conductivities are determined according to temperature and Ce^{3+} concentration by ref. 28, and the total conductivity σ is thereafter calculated by the brick-layer model. For c_{GB} above 50%, the conductivity is extrapolated from the original dataset. The computed σ values for each condition are plotted, as a function of c_{GB}, in Figure S7, and compared to the bulk CeO_2 conductivity. The limit of low grain boundary concentration (where $c_{GB} = c_{film\ bulk}$ and $\ell'_{GB} = t_{grain}$) corresponds to Ce^{3+} distributed uniformly across the sample, whereas the limit of high grain boundary concentration (where c_{GB} = 100% and $\ell'_{GB} = \ell_{GB}$) represents a maximally localized grain boundary reduction effect.

We find, somewhat counterintuitively, that the expected conductivity enhancement decreases monotonically with greater localization of excess Ce^{3+} to the grain boundaries. This can be understood on the basis that electronic conductivity in ceria, as a function of Ce^{3+} concentration, rises steeply at low concentrations before leveling out at values close to the spatially-averaged concentrations in the film ($c_{film\ bulk}$) and ultimately decreasing with concentration above ~25% Ce^{3+} [4]. Thus Figure S7 shows, for a range of realistic Ce^{3+} distributions, that relatively little conductivity enhancement is predicted from grain

boundary reduction, particularly in conditions #2 and #3, as long as the assumption of a fixed electronic mobility holds.

Tables & Figures

Table S1: Fitting results by the simple LC model ("LC only") and by the model including a self-absorption adjustment ("LC + SA") on all experimental XANES data. The "LC + SA" model is used for all analysis in this study.

Condition	Sample	Measurement type	Fitting model	R^2	c' (%)
#1	NanoX	Full-film (α = 9.5°)	**LC + SA**	**0.9998**	**2.1 ± 0.6**
			LC only	0.9988	3.4 ± 0.9
#2	NanoX	Full-film (α = 9.5°)	**LC + SA**	**0.9994**	**9.7 ± 1.0**
			LC only	0.9983	10.9 ± 1.0
	SingleX	Full-film (α = 9.5°)	**LC + SA**	**0.9999**	**4.7 ± 0.4**
			LC only	0.9998	5.0 ± 0.3
	SingleX	Surface (α = 0.23°)	**LC + SA**	**0.9693**	**56 ± 3**
			LC only	0.9328	62 ± 5
#3	NanoX	Full-film (α = 9.5°)	**LC + SA**	**0.9984**	**15.1 ± 1.5**
			LC only	0.9976	16.0 ± 1.2

Figure S1: Atomic force microscopy (AFM) height map of the nanocrystalline CeO_2 sample, measured after the XANES experiment. The root-mean-square roughness is 1.6 nm. This AFM image is characteristic of the sample's surface morphology, and no apparent evidence of (micro)porosity is observed.

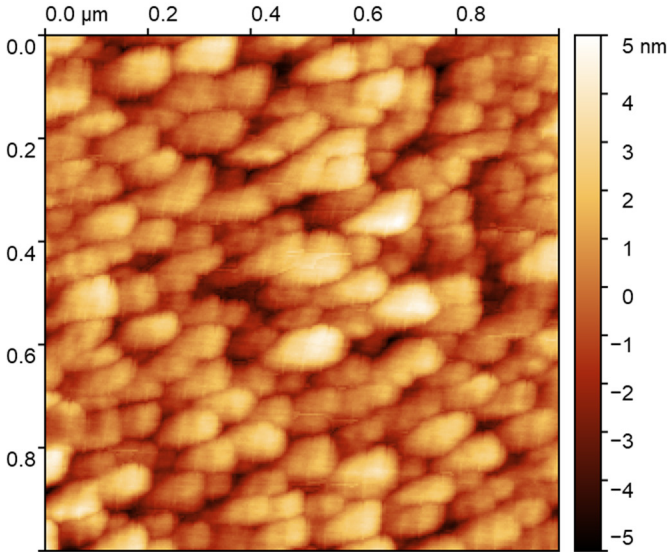

Figure S2: Specular X-ray reflectivity of the nanocrystalline CeO_2 film, measured after the XANES experiment, and best-fit curve using a two-layer (substrate and film) complex scattering length density (SLD) model. The SLD of the YSZ substrate was fixed at its theoretical value and the film thickness was fixed at 315 nm, the value measured by ellipsometry. From the fitted SLD of the film layer, the relative film density is $(\mathrm{Re}[SLD_{film,experiment}]/\mathrm{Re}[SLD_{CeO2,theoretical}])\times 100\% = 99\pm 5\%$. This is consistent with a dense polycrystalline sample with little or no porosity on a volumetric basis.

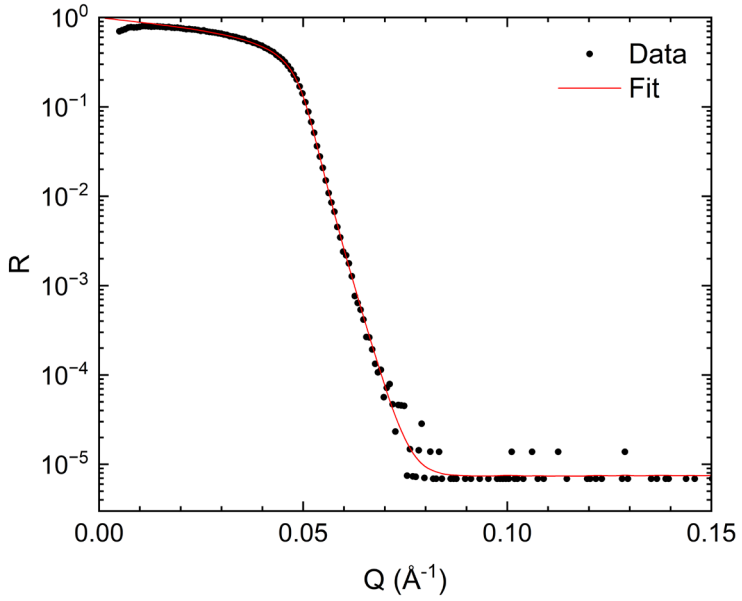

Figure S3: X-ray diffractometry (Cu K_α source, λ = 1.541 Å) of the single-crystal CeO_2 (100) film: **(a)** specular XRD (2θ scan), showing the presence of only CeO_2 and YSZ (substrate) reflections for the expected orientation, and **(b)** rocking curve (ω scan) at the CeO_2 200 reflection. The FWHM of the rocking curve is 0.273°, which indicates a high degree of (single-)crystallinity for an epitaxial film.

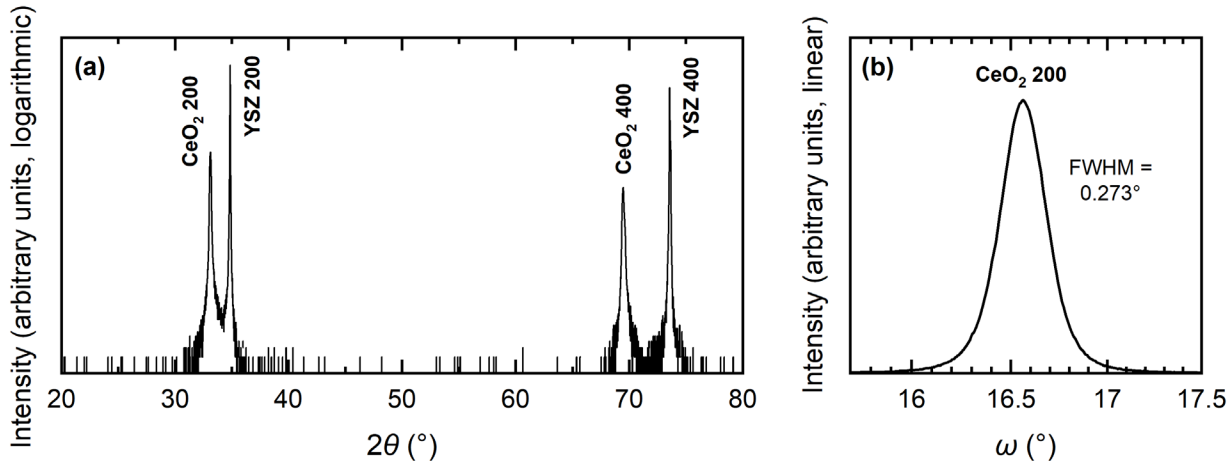

Figure S4: Characteristic AFM height map of the single-crystal CeO_2 sample. The root-mean-square roughness is 0.57 nm.

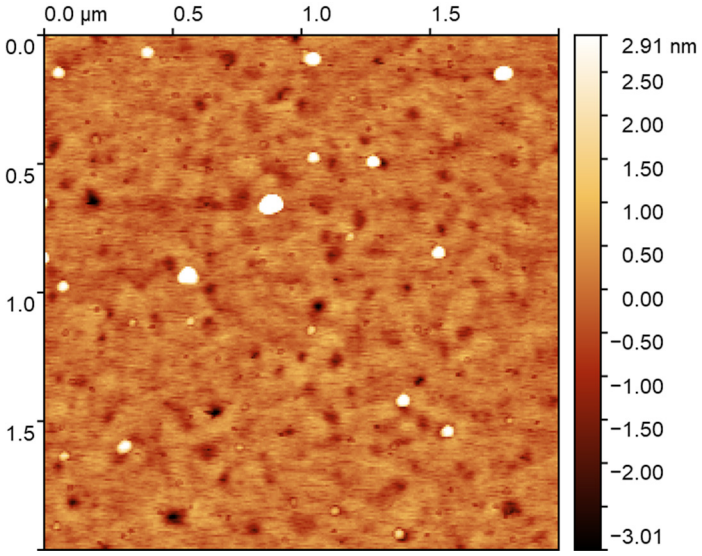

Figure S5: Fitting results by the simple LC model ("LC only") and by the model including a self-absorption adjustment ("LC + SA") on selected experimental data: **(a)** surface XANES (α = 0.23°) of single-crystal CeO_2 in condition #2 (Figure 2.e), and **(b)** full-film XANES (α = 9.5°) of nanocrystalline CeO_2 in condition #2 (Figure 2.b). The "LC + SA" model is used for all analysis in this study.

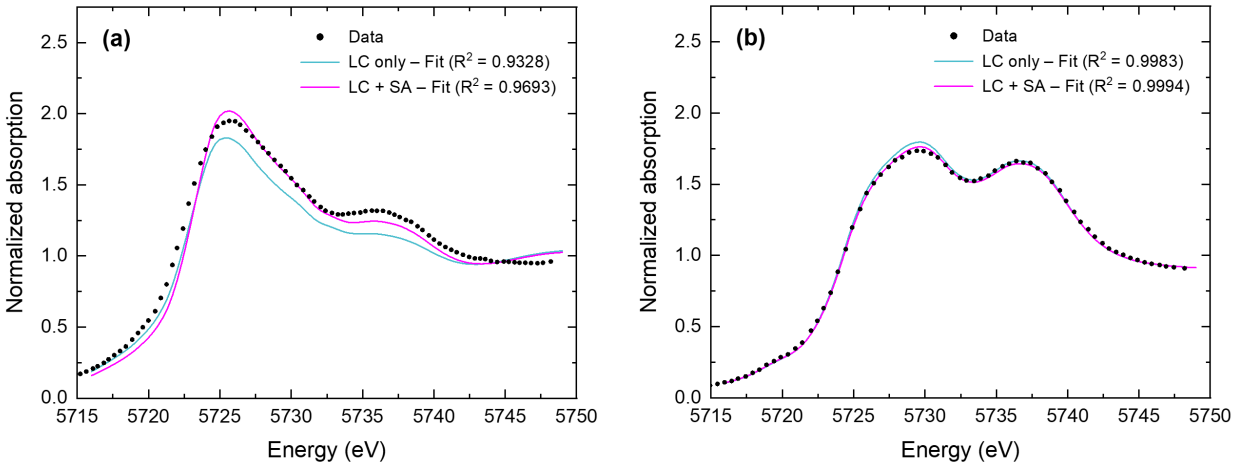

Figure S6: Analysis of residuals from linear combination (LC) fitting of XANES spectra. The dependence of residuals on Ce^{3+} content (c') is assessed by considering the four spectra collected at 845 °C (Figure 2.b-e). Of these four, the full-film measurement of the single-crystal film (Figure 2.d) has the lowest c' value (4.7%) while the surface measurement of the single-crystal film (Figure 2.e) has the highest c' value (55.7%). Linear combinations of residuals from these two measurements are here compared to the residuals from the other two measurements at 845 °C: **(a)** full-film XANES of nanocrystalline CeO_2 under condition #2 (Figure 2.b), and **(b)** full-film XANES of nanocrystalline CeO_2 under condition #3 (Figure 2.c). In each case, the fitting residuals are reproduced from Figure 2 (black) and plotted alongside the linear combination of residuals described above (red) according to the c' value for each measurement (9.7% and 15.1%, respectively). The rough agreement between the true residuals and the calculated linear combinations here suggests a shared origin of residuals that is linearly dependent on c', which is consistent with the hypothesis that most of the discrepancy between experimental XANES data and fitted curves is due to the imperfect nature of the Ce^{3+} reference spectrum.

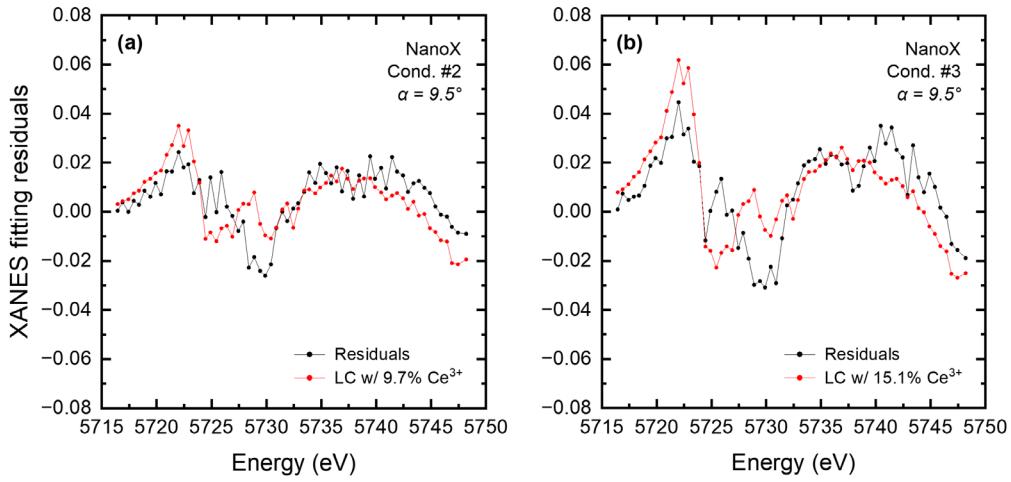

Figure S7: Estimation of total conductivity in nanocrystalline ceria treated with a brick-layer model in which the grain boundary Ce^{3+} concentration (c_{GB}) and grain boundary width (ℓ'_{GB}) are co-varied to produce the macroscopically observed total Ce^{3+} concentration ($c_{film\ bulk}$). Conductivity values were computed using data from ref. 28, and those for c_{GB} above 50% are obtained by extrapolation from the original dataset.

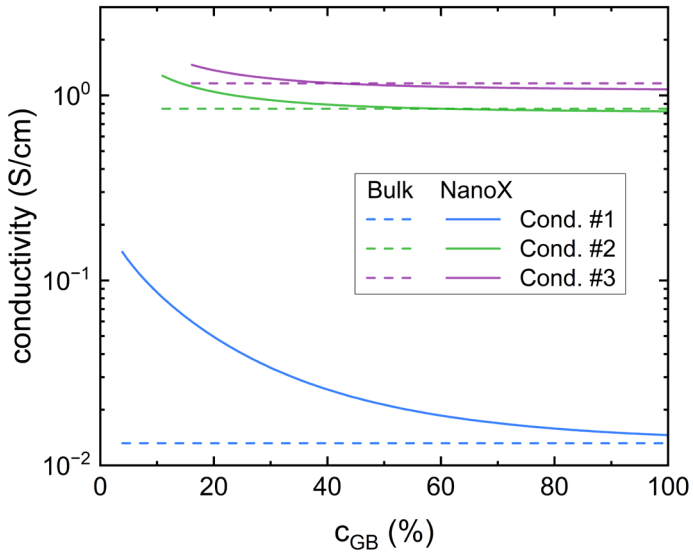

References

1. S. L. Moffitt, Q. Ma, D. B. Buchholz, R. P. H. Chang, M. J. Bedzyk, T. O. Mason, *J. Phys.: Conf. Ser.* **2016**, *712*, 012116.
2. P. Pfalzer, J.-P. Urbach, M. Klemm, S. Horn, M. L. denBoer, A. I. Frenkel, J. P. Kirkland, *Phys. Rev. B* **1999**, *60*, 9335.
3. R. C. Lye, J. C. Phillips, D. Kaplan, S. Doniach, K. O. Hodgson, *Proc. National Acad. Sci.* **1980**, *77*, 5884.
4. H. L. Tuller, A. S. Nowick, *J. Phys. Chem. Solids* **1977**, *38*, 859.
5. R. J. Panlener, R. N. Blumenthal, J. E. Garnier, *J. Phys. Chem. Solids* **1975**, *36*, 1213.